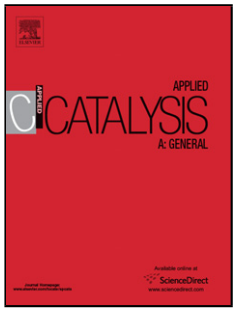

Title: In-situ XAS and FTIR studies of a multi-component Ni/Fe/Cu catalyst for hydrogen production from ethanol

Authors: A. Kumar J.T. Miller A.S. Mukasyan E.E. Wolf

PII: S0926-860X(13)00430-4
DOI: http://dx.doi.org/doi:10.1016/j.apcata.2013.07.032
Reference: APCATA 14348

To appear in: *Applied Catalysis A: General*

Received date: 26-4-2013
Revised date: 10-7-2013
Accepted date: 14-7-2013

Please cite this article as: A. Kumar, J.T. Miller, A.S. Mukasyan, E.E. Wolf, In-situ XAS and FTIR studies of a multi-component Ni/Fe/Cu catalyst for hydrogen production from ethanol, *Applied Catalysis A, General* (2013), http://dx.doi.org/10.1016/j.apcata.2013.07.032

Ethanol decomposition of Ni/Fe/Cu multicomponent catalyst

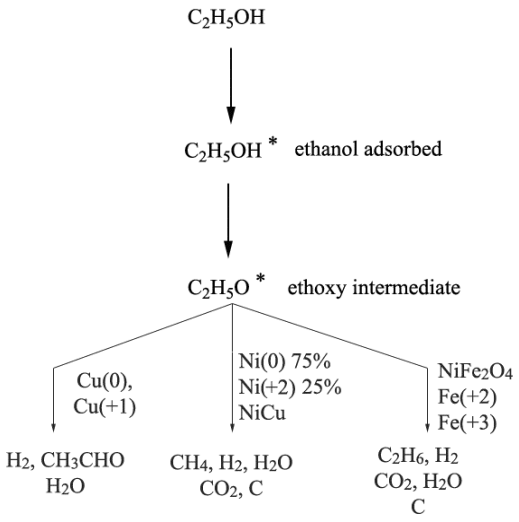

An active catalyst for ethanol decomposition reaction, containing nano-composites of Ni/Fe/Cu was synthesized using combustion based techniques. Different characterization results indicate that the segregated phases were active at different temperature ranges resulting in gradual change the product selectivity with temperature.

- NiFeCu catalyst appears homogeneous at the mesoscale but highly heterogeneous at the nanoscale.
- Cu oxidation state changes upon exposure to ethanol but Ni remains 75% reduced without further changes in oxidation state during reaction.
- Iron is not present in metallic form under any of the conditions used.
- XPS results indicate the enrichment of surface by Fe and Cu during the reduction.
- IR results show changes in the amount and type of adsorbed species with temperature and correlates with the active role of each metal at a given temperature.

In-situ XAS and FTIR studies of a multi-component Ni/Fe/Cu catalyst for hydrogen production from ethanol

A. Kumar[1,3], J. T Miller[2], A. S. Mukasyan[1], E. E. Wolf[1]*

[1]Chemical and Biomolecular Engineering Dept. University of Notre Dame, Notre Dame, IN 46556; [2] Chemical Sciences Div. Argonne National Laboratory, Argonne, Ill, [3]

Abstract

Multicomponent catalysts containing Ni, Fe, Cu active for ethanol reforming reactions, prepared by solution combustion synthesis are characterized by multiple techniques such as ex-situ XRD, XPS, and in-situ XAFS and FTIR. XRD results indicate copper to be present in the reduced state as Cu-Ni bimetal while nickel and iron are observed to be partially in a spinel $NiFe_2O_4$ structure. In-situ XANES and XAFS analysis show a change in Ni, Fe and Cu oxidation states during reaction. Cu, which was fully reduced before reaction, became partly oxidized upon exposure to ethanol and oxygen. Ni is mostly (75%) reduced and does not seem to change its oxidation state during the reaction. Fe is not present in metallic form after reduction and during the reaction, but some change in the oxidation state from Fe(II) to Fe(III) occurred during the reaction. XPS and SEM images indicate the formation of carbon filament on the spent catalyst. XPS results also indicate the enrichment of surface by Fe and Cu during the reduction of the catalyst. Based on the activity and characterization results obtained, and literature review, the role of predominant phases during ethanol decomposition reaction is proposed.

[3] Current location: Department of Chemical Engineering, Qatar University, Doha, P. O. Box 2713, Qatar

1. Introduction

1.1 Combustion synthesis:

Combustion synthesis (CS) is an attractive technique for materials synthesis on account of being simple, economical, fast and energy efficient. This simplicity and flexibility to synthesize a wide range of materials has led to an increased research interest as indicated by the increase in the publications on CS [1, 2]. The conventional solid-solid CS can be broadly classified into two types based on the way combustion reaction takes place. The combustion reaction can proceed as a self-sustained propagating reaction front after local ignition of the reactive solid form, or it can be combusted simultaneously all over the volume by using an external uniform heating source. The former method is known as Self-Propagating High-Temperature Synthesis (SHS) and the later as Volume Combustion Synthesis (VCS). Recent innovations have led to the use of CS in fluid phases such as solution combustion synthesis or SCS [3].

Among the above-mentioned methods, solution combustion synthesis, due to its ability to produce nano-materials, has recently gained attention and it is being applied to diverse areas of materials synthesis such as pigments, catalysis, electronic and magnetic materials, drug delivery etc [1, 2, 4]. SCS is considered as a redox reaction consisting of oxidizing agents (e.g. metal nitrates) and reducing agents (e.g. glycine, urea, hydrazine etc), also referred as fuel. The exothermic reaction between metal nitrates and the fuel provides the energy required for sustaining the combustion synthesis reaction without adding external energy. Furthermore, the energy released is high enough to evaporate volatile compounds and calcine the products formed leading to the formation of crystalline phases. Because the combustion reaction rate is very high, the crystallites formed do not have enough time to sinter, leading to the formation of nano-powders with higher surface area than obtained from conventional synthesis. Thus, SCS can

yield highly pure, crystalline materials with high surface area in a single step synthesis without requiring additional thermal treatments. In our previous work with methanol partial oxidation [5], we compared the co-precipitation vs CS preparation and found the later more active. Cu/Zn catalyst prepared by co-precipitation is reported to have a surface area of 17 m^2/g [5], whereas the catalysts prepared by combustion methods have area as high as 31 m^2/g [6]. Therefore in this work we focused mainly on the CS preparation. Work is underway comparing various methods of preparation on supported catalysts for ethanol decomposition.

The CS reaction between metal nitrates and glycine, used as fuel, can be represented by the following widely accepted scheme:

$$M^{v}(NO_3)_v + (\frac{5}{9}v\varphi)CH_2NH_2COOH + v\frac{5}{4}(\varphi - 1)O_2 \rightarrow M_vO_{\frac{v}{2}}(s) + (\frac{10}{9}v\varphi)CO_2(g) + \frac{25}{18}v\varphi H_2O(g) + v(\frac{5\varphi + 9}{18})N_2(g) \quad (1)$$

where M^v is a ν-valence metal. The parameter φ, the fuel to oxidizer ratio, is defined such that $\varphi = 1$ corresponds to a stoichiometric oxygen concentration, meaning that the initial mixture does not require atmospheric oxygen for complete oxidation of the fuel, while $\varphi > 1$ (<1) implies fuel-rich (or lean) conditions.

According to the above scheme, (Eq. 1), SCS can be used for the synthesis of metal oxides. Recent publications from our group [7-10] demonstrated that controlling φ during SCS one can synthesize reduced metals nano-powders as well (e.g. Ni, Cu rather than NiO, CuO). A reaction pathway was proposed to describe the controlled synthesis of different phases [9, 10]. The active solution containing a metal nitrate and glycine can be impregnated on a thin media (e.g. cellulose paper, carbon nano-tubes or graphite sheet etc.) before combustion synthesis to facilitate the cooling of the products obtained after CS [11-13]. This fast reaction and cooling, and the unique microstructure of the products, results in finer particles with higher surface area

than calcined oxides, which has potential for catalytic applications, as shown by previous results and model studies [12, 13].

This study complements our previous work on the synthesis and activity studies of multicomponent Ni/Fe/Cu based catalyst for hydrogen production from ethanol using SCS [14] which showed, $Ni_1Fe_{0.5}Cu_1$ to be the optimum catalyst composition among the several catalysts investigated for hydrogen production from ethanol partial oxidation and decomposition reactions. The focus of this work was to understand the role of individual metals in such complex multicomponent system rather than following an activity–selectivity optimization scheme by combinatorial compositional changes of the various components as previously reported. Ethanol's decomposition products were measured in detail on individual metals/oxides (Ni, Cu and Fe) as well as on the most active and selective multicomponent catalyst, $Ni_1Fe_{0.5}Cu_{1,}$ previously studied [14]. This paper attempted to correlate the activity of each component with its oxidation state, and in the differences in such results under *in-situ* conditions, without reaction, and under *operando* conditions i.e. in the presence of the reaction.

As stated earlier, SCS has numerous advantages over other catalyst preparation methods, such as co-precipitation that requires separation of the products after precipitation followed by calcination, which leads to sintering. As indicated by equation (1), except for the metal oxide product, all other products are gas phase products, which can be controlled by varying the parameter φ. The gases generated during CS form micro-channels on the solid products as they are released during reaction, thus contributing towards the porosity of the material synthesized, potentially leading to high surface area.

1.2 Ethanol reforming:

As the research interest on the fuel cells technology rises, the need for a pure hydrogen supply is also rising. Hydrogen can be abstracted from many hydrogen-containing precursors, and among them light alcohols (e.g. methanol, ethanol), are attractive renewable sources as they can be produced from corn stover [15] and other biomass byproducts [16]. The main routes for hydrogen generation from ethanol and the corresponding heat of reaction are as follows:

Ethanol Dehydrogenation and Decomposition:

$$C_2H_5OH \rightarrow CH_3CHO + H_2 \qquad -\Delta H^0_{298} = -68 KJmol^{-1} \qquad (2)$$

$$C_2H_5OH \rightarrow CH_4 + CO + H_2 \qquad -\Delta H^0_{298} = -49 KJmol^{-1} \qquad (3)$$

Ethanol Steam Reforming:

$$C_2H_5OH + 3H_2O \rightarrow 2CO_2 + 6H_2 \qquad -\Delta H^0_{298} = -174 KJmol^{-1} \qquad (4)$$

Ethanol Partial Oxidation:

$$C_2H_5OH + \frac{3}{2}O_2 \rightarrow 2CO_2 + 3H_2 \qquad -\Delta H^0_{298} = 509 KJmol^{-1} \qquad (5)$$

Ethanol steam reforming (ESR) is a highly endothermic reaction and requires steam to sustain the reaction. Ethanol decomposition (ED) is less endothermic than ethanol steam reforming, whereas ethanol partial oxidation (EPOx) is exothermic and releases energy during reaction. We previously studied the ED and EPOx reactions on Ni/Fe/Cu based catalysts on account of lesser energy requirements for hydrogen production. A review of the previously used catalysts for ethanol reforming is described in our previous paper [14]. On the basis of literature results, we selected Ni, Fe and Cu for the synthesis of multicomponent catalysts using combustion synthesis. Activity results from a family of such catalysts using a high throughput

approach showed that a $Ni_1Fe_{0.5}Cu_1$ catalyst gave the highest activity and selectivity among a limited series of catalyst studied.

2. Experimental

2.1 Catalyst synthesis

Aqueous solutions of metal nitrates (Alfa Aesar) $M^v(NO_3)_v \cdot xH_2O$ (where Me = Ni, Cu, Fe) and glycine ($C_2H_5NO_2$, as fuel) were used to synthesize catalysts in volume combustion synthesis (VCS) mode by forming a sol-gel of the precursors and fuel. The amounts of precursor materials were calculated based on the production of 3g of catalyst. These precursors were dissolved in 75ml of deionized water in a 400ml beaker. In the sol-gel VCS method the beaker containing the homogeneous solution of metal nitrates and fuel is heated over a hot plate until the sol-gel solution reaches the ignition temperature after evaporation of water. The fuel/oxidizer ratio φ, has been maintained at 1.75, which is the optimized value obtained from our previous studies [9] for the production of pure metals using combustion synthesis. Once ignited, the reaction proceeds very fast, which can lead to either an explosive combustion mode or to the self-propagating mode (SHS) mode inside the beaker itself. After synthesis, the resulting powders were milled using a planetary ball mill (Retsch PM 100) at 650 rpm for two minutes to get a mixture with uniform particle size. The ratio of catalyst sample and milling balls was kept at 1:2 in all the cases.

2.2 Catalyst characterization

Multiple techniques were used to characterize the Ni/Fe/Cu catalyst. XPS and XRD methods were used to determine elemental surface concentrations and identification of the bulk phases respectively. XANES and EXAFS experiments were conducted to determine oxidation states of

Ni, Fe and Cu under different reaction conditions. *In-situ* DRIFT studies were performed to get information about the adsorbed intermediates on the surface of the catalyst. The catalytic activity and selectivity data were published in our earlier paper [14]. The hydrogen selectivity reported is defined as the amount of hydrogen produced to the maximum amount of hydrogen that could have been produced with the reacted ethanol.

$$S_{H_2} = \frac{H_2\ Produced}{3 \times (Ethanol\ converted)} \times 100$$

2.2.1 XRD, SEM and TEM measurements:

XRD measurements were carried out in air at room temperature in an X-ray diffractometer (Scintag Inc) using Cu-Kα radiation of 1.54056 Å wavelength. The powdered samples were loaded on an amorphous glass sample stage to avoid signals from the sample holder itself. Powder microstructures were imaged using a field emission SEM (Magellan 400 FEI) at Notre Dame Integrated Imaging Facility (NDIIF). Transmission electron microscopy images were collected using Titan 80-300, which is capable of providing atomic level imaging and is equipped with nano-scale resolution EDS (energy dispersive spectra) facility.

2.2.2 X-ray photoelectron spectroscopy.

X-ray photoelectron spectra measurements were obtained using a Kratos XSAM-800 system using Mg-Kα radiation at 1253.6 eV and an electron takeoff angle at 90° (sample normal). Powder samples were mounted on sample stubs with double sided conductive carbon tapes. The peak areas were analyzed using the CasaXPS software package with relative sensitivity factors obtained from Kratos XSAM library. These results were used to estimate the surface concentration of different elements and their oxidation states under vacuum using carbon

as standard for calibrating the peak locations. Samples were reduced ex-situ at 300ºC for 1 hour under continuous hydrogen flow. The reduced samples were transferred to the XPS sample transfer chamber using a glove bag. A sealed reactor containing the reduced catalyst was placed inside a glove bag, which was mounted on the door of transfer chamber and purged multiple times with Ar to eliminate residual air that could oxidize the sample before opening the reactor and transferring the sample. The same procedure could not be used with the used samples that were exposed to air after removal from the reactor.

2.2.3 TPR experiments:

The TPR experiments were conducted on a catalyst characterization unit of our own design equipped with a flow reactor connected to a 6-port sample valve for injecting pulses, a thermal conductivity detector, and automated flow and temperature controllers. Prior to a TPR run, each catalyst (approx 100 mg) was oxidized using 20% O_2 in Ar, flowing at 50cc/min while being heated from room temperature to 300ºC in 30min then kept at this temperature for an hour. After that, the flow was switched to pure He/Ar to flush the system while it cools down to room temperature. For TPR measurements a carrier gas containing 5% H_2 in Ar flows through one side of the TC cell before entering the flow reactor containing the catalyst sample. The reactor effluent is connected to a water trap to adsorb or condense the water formed during reduction. The water-free effluent gas flows over the sample side of the TC cell allowing it to detect any loss in hydrogen that may occur due to reduction of the catalyst.

2.2.4 X-ray absorption studies:

The XANES and EXAFS experiments were carried out at the Advanced Photon Source (APS) facility at the Argonne National Laboratory (ANL). The spectra were obtained in transmission mode at the sector 10 MRCAT (Material Research Collaborative Access Team)

beam line 10-BM, equipped with a bending magnet (BM). This beamline has a double crystal Si(111) monochromator to select the incident x-ray photon energy. A detuning of 50% was used to accomplish the rejection of higher order harmonics in the beam. Self-supported catalyst wafers were prepared by pressing the sample, diluted by silica, into a cylindrical holder with multiple channels that can contain up to six catalysts at a time. The dilution of a sample with silica and the amount of diluted sample to make wafers were adjusted to get the optimized absorption edge height $\chi(E)$ to about 1 unit. In Cu, Ni, Fe samples, the dilution ratio varied between 1:2 to 1:7 (wt sample: wt silica) and the amount required for wafer preparation varied from 7mg-15mg of the diluted sample. The 6-channel multiple sample holder was placed in the center of a quartz tube of 0.75" ID and 18" length. The tube has fitting arrangements at both ends with an inlet and outlet for the reactant gases to flow through the reactor, and an inlet for a K-type thermocouple to measure the sample temperature. The reactor tube end fittings have openings at both ends that were covered with polyimide film providing a window to allow transmission of the X-ray beam and to seal the tube. An electrical furnace with a temperature control heated the catalysts to set the pretreatment and reaction temperatures. This set up allowed us to obtain X-ray absorption (XAS) spectroscopy measurements during *in-situ* and under reaction conditions i.e. *in operando* mode under the following conditions:

A: In air at room temperature; B: *In-situ* reduced sample at room temperature; C: *Operando* at 270 ºC during reaction (ethanol decomposition and ethanol partial oxidation reaction).

The sample was first reduced at 300 ºC for 1 hr in a 5% H_2 (balance He) stream flowing at 50 cc/min in a hood located outside the x-ray beam station to optimize utilization of the beam line. After reduction, the sample was cooled down in the gas flow to room temperature, then the flow was stopped and the inlet and outlets valves were closed to isolate the reactor from the

atmosphere and avoid air contact. The gas lines were disconnected and the reactor was transferred to the beam line and reactant gas lines were reconnected. The fitting tubes and valves were purged before flowing reactant gases inside the reactor. XAS spectra were first obtained at room temperature on the reduced samples then the reactor temperature was raised from room temperature to 270 ºC under the continuous flow of reactants. *Operando* measurements were taken at this temperature at the same conditions used for ethanol decomposition and ethanol partial oxidation reaction. Standards for the reduced metals were obtained from metal foils (for Cu-Cu, Ni-Ni and Fe-Fe phase and amplitude parameters) and for the oxides using standard CuO, Cu_2O (for Cu-O parameters), NiO (for Ni-O parameters), FeO, Fe_2O_3 (for Fe-O parameters). The experimental data obtained is fitted to standard scattering equation to get the coordination numbers; inter-atomic distances etc. using standard WINXAS97 and ATHENA software. The Debye-Waller (DW) factor was obtained by fitting the spectra of the reduced sample at the 270 ^{o}C and at room temperature using reference spectra. The presence of an oxide fraction makes it difficult to calculate the nanoparticle size directly from the coordination number. Therefore, estimates were made by using the metallic fraction present in the XANES spectra of the nanoparticle. For example a XANES spectra at room temperature in air shows 75% metallic copper and 25% Cu(I) present in the catalyst nanoparticle. The actual Cu-Cu coordination used for size estimation was 11.5 (8.6/0.75). The % of each phase in the $NiFe_{05}Cu$ catalyst was estimated from the XANES spectra using a linear combination of the peak height over its value past the edge energy as obtained from the standards used [17].

2.2.5 Diffuse Reflectance Infrared Fourier Transform Spectroscopy (DRIFTS):

DRIFTS measurements were carried out in a Bruker FTIR spectrometer (Equinox 55) using a DRIFTS reaction cell (Harrick, HVC) with a flat ZnSe windows and a praying mantis

optical assembly (Harricks, 3-3S). The distance between the ZnSe window and the catalyst sample was kept at minimum to reduce the gas phase signals. The catalyst samples were diluted with fumed SiO_2 in a ratio of 1:2 to 1:4 to reduce IR absorption by the dark samples and enhance reflectance. Each sample was first reduced in-situ at 300ºC for 1 hour in a continuous flow of 30 cc/min containing 20% H_2 (balance He) gas. Thereafter, the system was purged with He (25 cc/min) at 300ºC for half an hour. Background spectra were taken first at different temperatures in continuous He flow.

Ethanol was introduced by directing the He through an ethanol bubbler kept at room temperature for 10 min during desorption studies. The system was purged with continuous He flow, while desorption spectra were taken at regular intervals. The ethanol decomposition reaction was studied under continuous flow of ethanol while increasing the temperature. Spectra were obtained using a MTC detector in the frequency range of 370– 4000 cm^{-1} with a resolution of 4 cm^{-1} by collecting 128 scans at a scan velocity of 3 K-Hz using a MTC detector.

3. Results and discussion

As described earlier all the catalysts in reference [14] were synthesized by using SCS method. The BET area of the synthesized catalysts varied from 11 m^2/g to 30 m^2/g. The BET area for $Ni_1Fe_{0.5}Cu_1$catalyst used for detailed characterization is 16 m^2/g.

3.1 XRD analysis:

XRD results (ex-situ in air at RT) in figure 1 shows diffraction peaks obtained after CS of the single metal nitrate-glycine system (Ni), the bi (NiCu) and the tri-metal nitrate-glycine ($Ni_1Fe_{0.5}Cu_1$) catalysts by adding $Cu(NO_3)_2$ and then $Fe(NO_3)_3$ to the $Ni(NO_3)_2$-glycine mixture and maintaining the same fuel to oxidizer ratio (φ = 1.75). The ratio, φ = 1.75, was optimized to

produce pure metal (Ni) and a (CuNi) alloy [13]. Maintaining the same ratio φ = 1.75 in presence of $Cu(NO_3)_2$ and $Fe(NO_3)_3$ gives CuNi (the CuNi[111] peak at 2θ=43.94, 51.19, 75.31) , pure Ni[111] (peak at 2θ=44.5, 51.84, 76.37) and $NiFe_2O_4$ spinel phases indicating that in the bulk of these catalysts, Cu is completely reduced, Ni partially reduced and Fe to be in oxide form (Fe_2O_3). There are many factors that affect the oxidation state of a synthesized catalyst. Copper exhibits three oxidation states during the CS process which gradually changes from Cu(II) to Cu(I) and then to Cu(0) as we move from φ value 0 to 3. Ni exhibits only two oxidation states and changes from Ni(II) to Ni(0) when φ is changed from 0 to 1.75. Both Ni and Cu have comparable affinity for oxygen (Cu-O and Ni-O comparable enthalpy of dissociation). The detailed mechanism that leads to reduction of these metals instead of the oxide phase predicted by Eq (1), is not known in detail and is under investigation, but it involves several intermediate decomposition reactions of the nitrates and glycine that yields reducing gases that lead to the metal phase. It appears that extra hydrogen is required to reduce Cu(I) to Cu(0) and thus a higher value of φ. As shown in the reference [9] using φ =1.75 yields Cu(I) and Cu(0) oxidation states and no Cu(II).

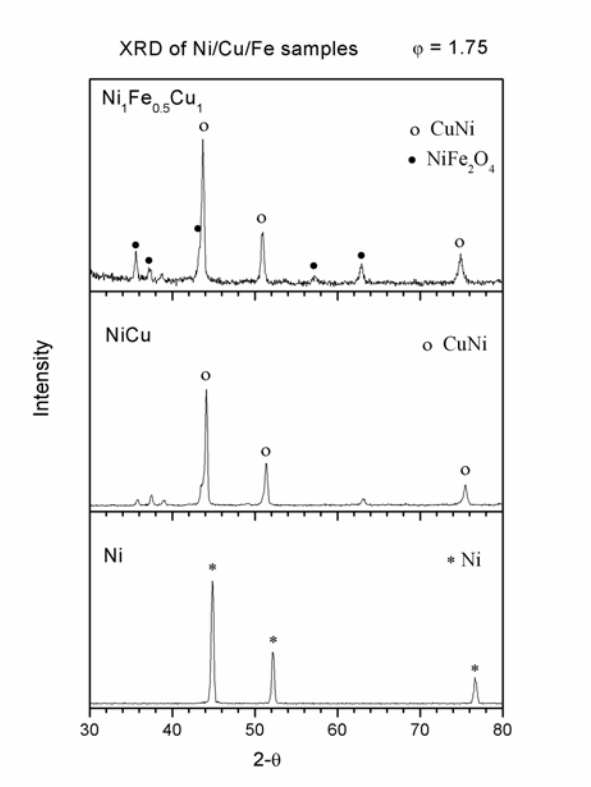

Figure 1: XRD results on the products from $Ni(NO_3)_2$-Glycine, $Ni(NO_3)_2$-$Cu(NO_3)_2$-Glycine and $Ni(NO_3)_2$-$Fe(NO_3)_3$-$Cu(NO_3)_2$-Glycine mixtures combustion

3.2 TPR analysis:

Figure 2 shows the TPR analysis conducted on Fe_2O_3, CuO, NiO and $Ni_1Fe_{0.5}Cu_1$ catalysts prepared by CS. Fe_2O_3 is the most difficult metal oxide to reduce, giving a peak for hydrogen uptake at 453ºC, most likely due to its partial reduction from Fe_2O_3 to FeO, with another peak appearing above 650ºC. CuO shows a peak for maximum hydrogen uptake at 250ºC while NiO reduces at a lower temperature than CuO at 237ºC. This could be due to the effect of the fuel to oxidizer ratio used which was optimized to φ=1.75 to produce pure Ni metal as compared to CuO and Fe_2O_3 where the same value of φ=1.75 results in metal-oxide phases for Cu. A higher value of φ=3.0 is required to produce pure Cu using combustion synthesis [10],

whereas Fe is more difficult to produce and may require the combustion synthesis to take place in an inert atmosphere, in addition of using a higher φ value. $Ni_1Fe_{0.5}Cu_1$ gives a first peak at 225ºC and another broader peak between 385ºC - 500ºC.

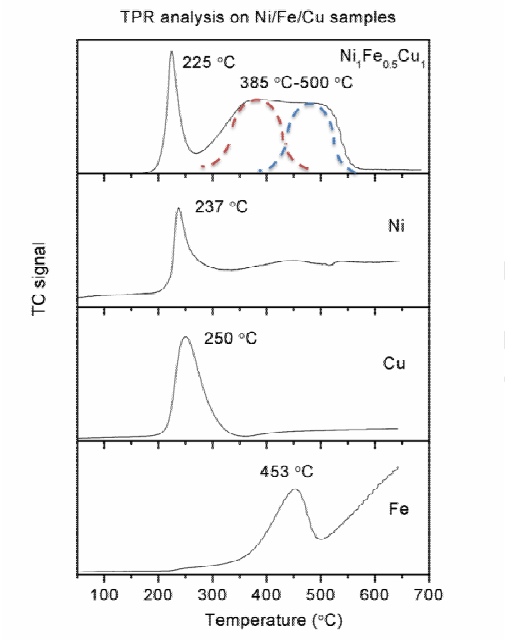

Figure 2: TPR analysis on Fe, Cu, Ni, and $Ni_1Fe_{0.5}Cu_1$ catalysts prepared by combustion synthesis

It is clear that the presence of Ni, Fe and Cu together increases the reducibility of Ni/Cu mixtures and decreases the reduction temperature to a lower value of 225ºC in comparison to 237ºC and 250ºC, as observed in pure NiO and CuO phases respectively. Fe_2O_3 also seems to reduce earlier in $Ni_1Fe_{0.5}Cu_1$ as the TPR profile becomes flat after 500ºC and there is no indication of a third peak around 650ºC as in the single Fe_2O_3 TPR profile. So the broader peak between 385ºC-500ºC could be a combination of two close peaks of Fe_2O_3. From the TPR analysis it can be concluded that the three metallic/oxide phases together makes the catalyst more reducible in comparison to each individual metal oxide phase. The metals and metal oxides present together not only effect the reducibility of the multicomponent catalyst, but these phases

313 also rearrange themselves during different treatments of the catalyst such as reduction and
314 exposure to ethanol etc. The actual surface concentrations of individual metals under vacuum
315 were determined by XPS as described below.

316 *3.3 X-ray photoelectron spectroscopy*

317 XPS results of the $Ni_1Fe_{0.5}Cu_1$ catalyst were determined after exposure to three different
318 states: in air, reduced state and after the ethanol decomposition reaction. Since the sample was
319 exposed to air after reaction, the XPS spectra of the used catalyst essentially matches the one of
320 the sample in air. Figure 3 shows the XPS spectra at energies corresponding to Cu 2p (fig 3a), Ni
321 2p (fig 3b) and Fe 2p (fig 3c) photoemission from the catalyst treated in air, reduced, and after
322 reaction. Apart from these peaks, carbon and oxygen peaks were also observed. Copper was
323 expected to be in the reduced state as the XRD results indicated. Surface oxidation from residual
324 atmospheric oxygen could not be avoided, however, as indicated by the shift in the Cu 2p peaks
325 towards a higher binding energy on the samples in air and after the reaction as compared to the
326 reduced sample, indicating the presence of Cu^{+2} oxidation state on the surface. Ni 2p peaks in air
327 and used samples are also shifted toward higher oxidation state than the reduced ones showing
328 that the surface oxidation differ from the bulk sample, which is mostly reduced, according to
329 XRD. The binding energy of the Fe 2p peaks does not change after reduction and is present in
330 the Fe^{+3} oxidation state. The separation between the 2p peaks of Ni, Cu and Fe is due to spin
331 orbital splitting.

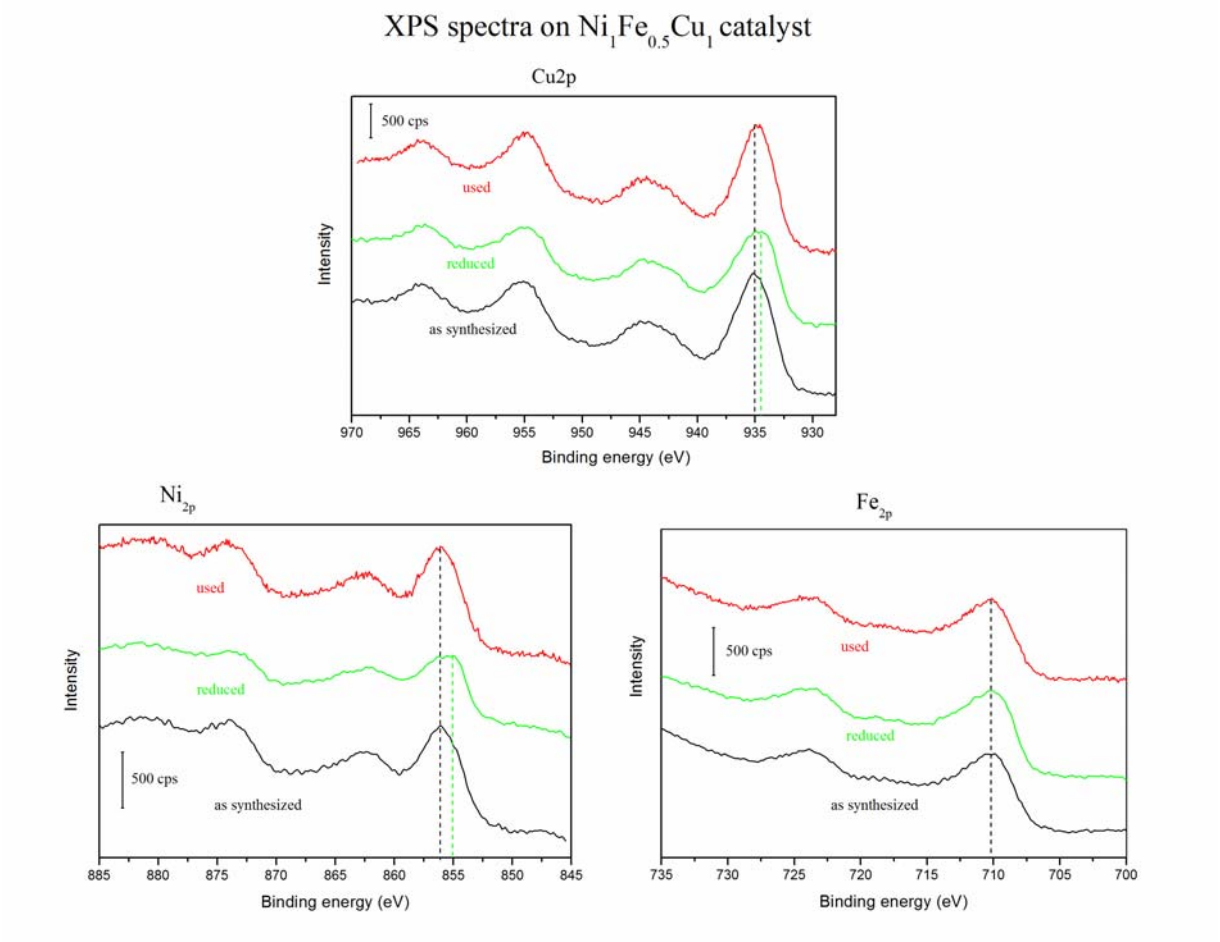

Fig 3: XPS spectra of $Ni_1Fe_{0.5}Cu_1$ catalyst in air, after reduction and after reaction (a) Cu_{2p} (b) Ni_{2p} and (c) Fe_{2p}

Table 1: Atomic ratio of Ni, Fe and Cu on the surface of $Ni_1Fe_{0.5}Cu_1$ catalyst

Total atomic ratio	**Fe/Ni**	**Cu/Ni**
$Ni_1Fe_{0.5}Cu_1$, **in air**	1.3	2
$Ni_1Fe_{0.5}Cu_1$, **reduced**	2.4	2.6
$Ni_1Fe_{0.5}Cu_1$, **after reaction**	1.2	2.1

Table 1 gives the atomic ratio of Ni, Cu and Fe relative to Ni near the surface region, (referred hereafter as surface) of the $Ni_1Fe_{0.5}Cu_1$ catalyst respectively. The relative concentrations of different elements are calculated based on the area of the XPS and the sensitivity factor for each element. Although the bulk catalyst was synthesized based on an atomic ratio of 1:0.5:1 of Ni:Fe:Cu, the surface composition of the catalysts exposed to air is different and contains Ni:Fe:Cu in 1:1.3:2 ratios, most of which are the oxides of the different metals. After reduction, Fe/Ni and Cu/Ni atomic ratios increase to 2.4 and 2.6 respectively. Surface reconstruction and composition are determined by the surface's Gibbs free energy. The oxide phases of Ni, Fe and Cu have significantly lower surface energies than their pure metallic phases and for this reason their metallic surfaces tend to form oxides when exposed to oxygen [18, 19]. The spinels (MN_2O_4, M_3O_4) have lower surface energy than the metals (M), rocksalt oxides (MO) and trivalent oxides (M_2O_3) [19]. This could be the reason why only pure Ni is obtained using combustion synthesis at an optimized fuel to oxidizer ratio of φ=1.75, whereas the same fuel to oxidizer ratio in the presence of Fe and Cu gives spinel ($NiFe_2O_4$) phases (see XRD pattern, fig 1). The surface goes back to its initial state after the reaction and exposure to air.

The XPS spectrum of the C1s photoelectrons (shown in supplementary figure S1) observed at 284.5 eV shows a large peak on the spent $Ni_1Fe_{0.5}Cu_1$ catalyst after a 40 hour time on stream at 400ºC. Ni and Fe, known for their activity towards C—C bond scission, are likely to be responsible for carbon formation. As previously reported [14], deactivation which reduces the catalyst hydrogen selectivity but not the conversion as a function of time on stream (TOS), could be attributed to the formation of carbon species altering the distribution of active sites. It is anticipated that at longer TOS the conversion will also decline. Activity experiments conducted

on individual metals [14], indicate no carbon formation on Cu only catalyst. Carbon formation has been reported on Ni, Fe, Co based catalysts [20] and it grows forming filament-like structures as shown in the SEM micrograph shown in figure 4a. A mechanism for the carbon filament formation and growth was proposed by Baker et. al [20] and later refined by others [21-23] wherein the metal particle grows at the top of the filament, which is consistent with the sustained conversion shown with TOS but the significant effect on the H_2 selectivity in favor of total oxidation.

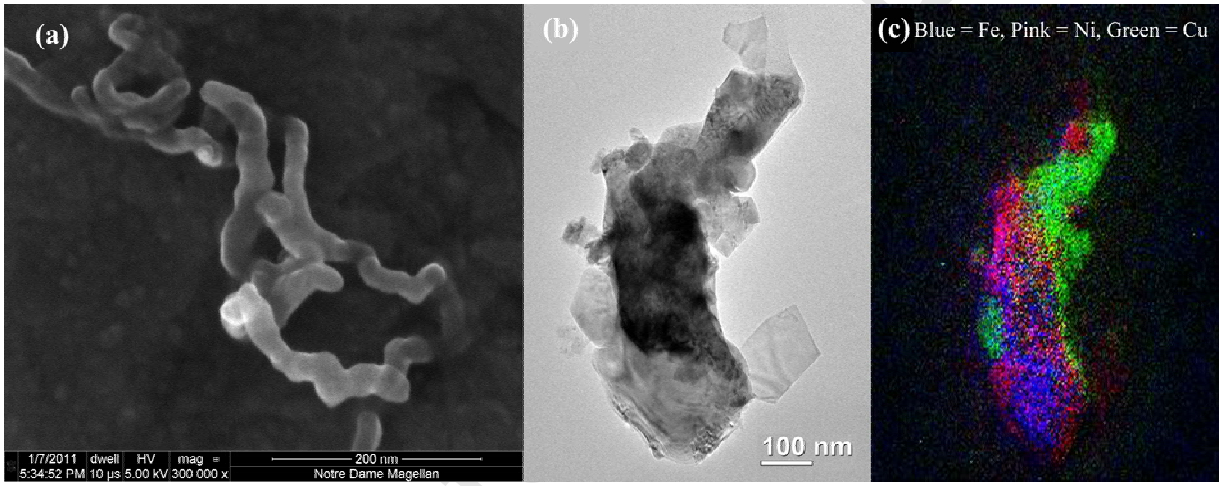

Figure 4: (a) SEM micrographs of carbon filaments on the surface of spent $Ni_1Fe_{0.5}Cu_1$ catalyst. (b) TEM image and (c) phase distribution using HRTEM on a $Ni_1Fe_{0.5}Cu_1$ catalyst.

XPS studies provide information about the surface concentrations under ultra-high vacuum condition, which is different than under reaction conditions, nonetheless the results indicate that on the reduced catalyst surface the various phases are in a different ratio than in the synthesized bulk catalyst. The bulk catalysts oxidation states, were studied under *in-situ* and *operando* conditions which are described later in the XAS section. A TEM image along with EDS is presented next to describe the phase distribution at nano-scale.

3.4 Transmission Electron Microscopy:

Figure 4b shows the results obtained on high resolution TEM. The catalysts particles are agglomerates of heterogeneous nanoparticles ranging from 10-100 nm size. The structure appears to be very non-uniform contrary to our expectations. As the solution combustion synthesis involves molecular level mixing of different metal nitrates and glycine, a homogeneous product with uniform properties is expected. Different phases are segregated around the bulk of the catalyst (fig 4c). This could be partly due to the difference in the solubility limits and precipitation of different components in a solution containing multiple salts. Although combustion synthesis is a fast process and mainly dependent on the ignition of the decomposition products of metal nitrates and glycine (ammonia and nitric acid), it is difficult to rule out any sort of precipitation for the fact that individual metal nitrates have different decomposition temperature and it is highly probable that solution reaches solubility limit just before its ignition. This heterogeneity is restricted to nanoscale only, as the EDS data obtained using LEO SEM (not shown), which gives information from ~1 μm depth, shows uniform distribution of all the phases. This heterogeneity at the nanoscale clearly explains the results obtained during ethanol reforming reaction [14]. Different segregated phases seem to dominate the product distribution at different temperature ranges resulting in a gradual shift in the product selectivity with temperature.

3.5 In-situ and operando XANES and EXAFS studies

The Ni edge XANES spectra in air, reduced, and under reaction, of the $Ni_1Fe_{0.5}Cu_1$ catalyst, are shown in figure 5. The trends in the Cu edge look similar to Ni edge, and the Fe edge spectra did not show much change in oxidation states. Ni edge results (figure 5) in

$Ni_1Fe_{0.5}Cu_1$, indicates that Ni is partially oxidized at room temperature with an estimated 58% NiO and only 42% Ni phase. The amount of Ni phase increases to 75% after reduction though it is still not completely reduced. Adding ethanol does not seem to affect the oxidation state of Ni as no changes in Ni phase is observed in presence of ethanol at 270°C, while the ethanol and oxygen together increase the Ni oxidation state as indicated in the supplementary table S1 where the fraction of pure nickel decreases to 70% from the initial value of 75% after reduction. It should be noted that these changes are time dependent and they initially take place in a few minutes but then they level off and remain nearly constant up to 40 mins. Limitations on beam line use prevented us to study changes at longer time on stream.

Results from the Cu edge are as follows: Cu was found to be partly in Cu(I) oxidation state in the $Ni_1Fe_{0.5}Cu_1$ catalyst at room temperature, in air, having an estimated 25%Cu(I) and 75%Cu(0). This partial oxidation of Cu could be a result of long-term exposure to air during sample preparation for XAS analysis. After reduction, the edge matches quite well with metallic Cu reference foil edge (Fig 5b), indicating complete reduction to metallic Cu(0) oxidation state. In the presence of ethanol at 270°C, a small change in oxidation state takes place and 15% of Cu(0) changes to Cu(I), whereas the oxidation state in the presence of both ethanol and oxygen, appears more pronounced giving 30% Cu(I), but in all the cases, a large fraction of Cu remains in the reduced state. Results from the Fe edge in air at room temperature indicate that the sample contains mainly Fe(+3) and some Fe(+2), giving an overall oxidation state of the entire sample to be 2.3 (Fig 5c). After reduction, some fraction reduces to Fe(+2), but the edge height is much higher than the reference Fe metal foil (Fig 5c), showing the absence of metallic Fe. At 270ºC, in presence of ethanol as well as in presence of ethanol and oxygen, only a minor change was

observed in the edge shape and height indicating that only small changes in the oxidation state of Fe occurs during exposure to the reaction mixture.

In addition to the XANES spectra, EXAFS spectra were taken at all the three, Cu, Ni and Fe edges, to study the change in oxidation states, and estimate the size of nano-particles (NP) and the coordination state of each element in $Ni_1Fe_{0.5}Cu_1$. The phase and amplitude files of the constituent phases in R (Fourier Transform) space from the EXAFS results can be fitted with the phase and amplitude files obtained from references (e.g. metal-metal and metal-oxygen) to obtain nearest neighbor and scattering distances. The Debye-Waller factors and energy corrections (E_0) used for fittings are listed in the tables provided in the supplementary file (Table S1-S3).

Table S1 summarizes the results obtained on the Ni edge for $Ni_1Fe_{0.5}Cu_1$ in different conditions. $Ni_1Fe_{0.5}Cu_1$ in air contains 42% Ni in reduced Ni(0) state which increases to about 75% Ni(0) metal after reduction, and in presence of ethanol at 270°C. In EtOH + O_2 at 270ºC, a slightly more oxidized NiO, by about 5%, is estimated from EXAFS fitting. Pre-treatment with EtOH (either with or without O_2) reduces the size of Ni nanoparticles to 2-3 nm whereas just after reduction in H_2 (at 300ºC) the nanoparticles were about 4-5 nm. It is interesting to note that the metal-metal bond distance is 2.53 Å, which is an indicative of Cu-Ni bimetallic particle. Ni-Ni scattering distances in Ni only catalyst is 2.49 Å, while Cu-Cu in Cu only catalyst is 2.55 Å. An alloy of Ni-Cu would have an intermediate bond distance.

Fourier Transform of the real (solid lines) and imaginary part (dotted lines) of the fitted $k^2 \cdot Chi(k)$ function of the EXAFS spectra of Ni-only catalyst reduced at 300ºC and the Ni foil are shown in the supplemental information, Figs S2a and S2b. The smaller size of the magnitude of FT indicates that the Ni nanoparticles are small and the imaginary part of the first shell and

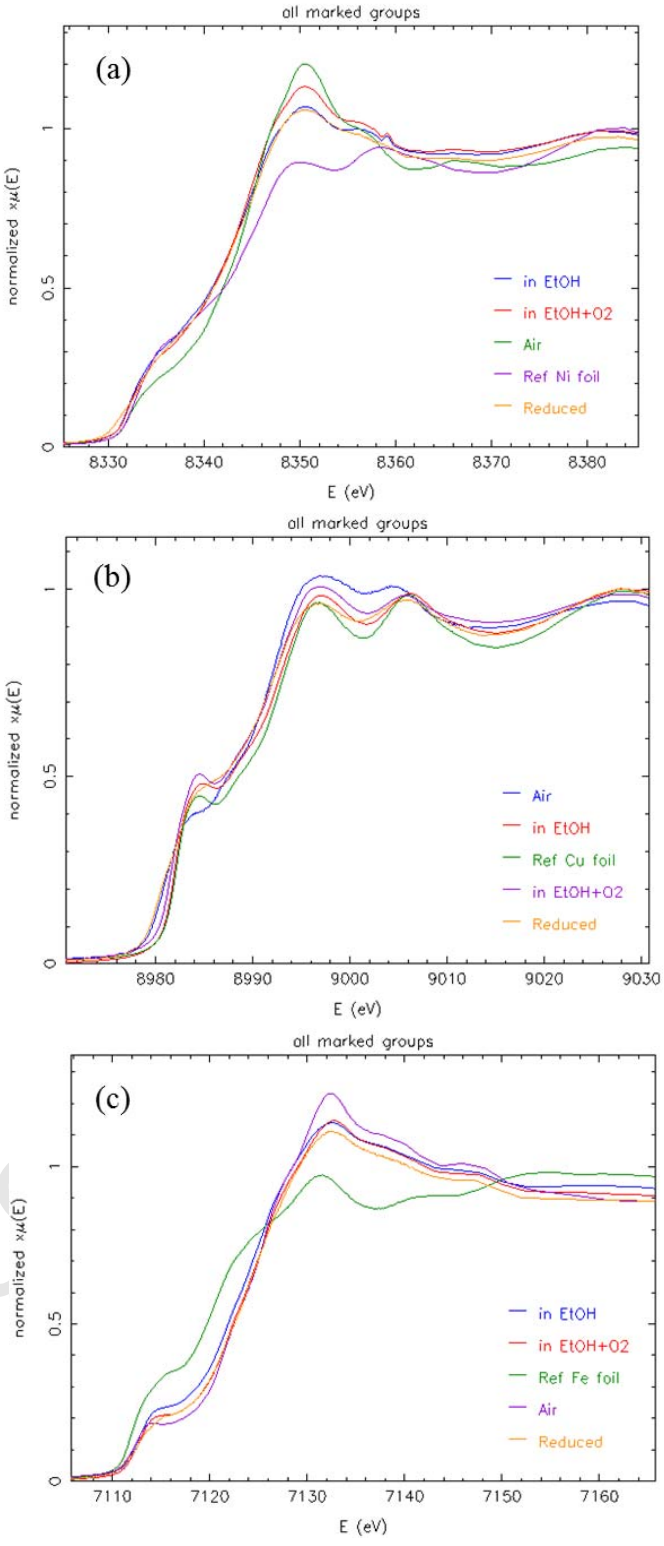

441

Figure 5: XAS spectra on $Ni_1Fe_{0.5}Cu_1$ catalyst; in air, reduced and during reaction, (a) Ni edge XANES, (b) Cu edge XANES and (c) Fe edge XANES

442

443 higher shells are identical to that of Ni foil, indicating identical bond distances of the Ni only
444 catalyst w.r.t. the Ni foil (Fig. S2a). A comparison between the FT of k^2·Chi(k) of Ni K-edge of
445 Ni-only catalyst and $Ni_1Fe_{0.5}Cu_1$ catalyst after reduction at 300ºC, shows a large shift in the
446 imaginary part of the FT for the $Ni_1Fe_{0.5}Cu_1$ catalyst indicating a different bond distance of 2.52
447 Å (Fig. S2b) than the reduced Ni-only catalyst. Since this value is in between the Cu reduced
448 bond distance (2.55 Å) and Ni (2.49 Å) it suggests that there is some intermediate degree of
449 phase distribution or alloying between Cu and Ni and the presence of an alloy is expected rather
450 than pure Cu or Ni phases.

451 Figure 6a shows the FT of k^2·Chi(k) of the Ni edge of the $Ni_1Fe_{0.5}Cu_1$ catalyst after
452 reduction and during the ethanol decomposition reaction at 270ºC. It is clear that these two peaks
453 fit very well indicating similar percentage of reduction in both conditions. During ethanol
454 decomposition, the reducibility of Ni nanoparticles (NP) does not change and remain nearly
455 constant at 75%. However the smaller magnitude of the FT indicates the presence of smaller NP
456 during ethanol decomposition reaction.

457 Figure 6b shows the magnitude of the Fourier Transform of the k^2·Chi(k) function of the
458 EXAFS spectra of the Cu K-edge on the $Ni_1Fe_{0.5}Cu_1$ catalyst after reduction and during ethanol
459 decomposition at 270ºC, along with results from a Cu foil used as reference. Cu in the
460 $Ni_1Fe_{0.5}Cu_1$-air catalyst is 25% Cu(+1) and 75% Cu(0) metallic (Table S2). The smaller size of
461 the magnitude of k^2·Chi(k) in presence of ethanol indicates a smaller particle size than after
462 reduction in H_2. Upon reduction, Cu is fully reduced and the nanoparticles are larger than 9 nm,
463 as determined by an empirical relationship obtained by fitting the particle size and the
464 coordination number [24-26]. These estimates, however, may not be accurate at these large
465 sizes, i.e., at N greater than about 11. It is clear from fig 6b that most of the Cu in ethanol

466 decomposition is in the reduced form but with formation of significantly smaller Cu
467 nanoparticles, ~ 3 nm. These results suggest that during oxidation-reduction–reaction
468 environments there is a significant structural transformation of the Cu-containing phases and a
469 phase segregation of Cu_2O phase is likely to happen from NiCu bimetallic phases

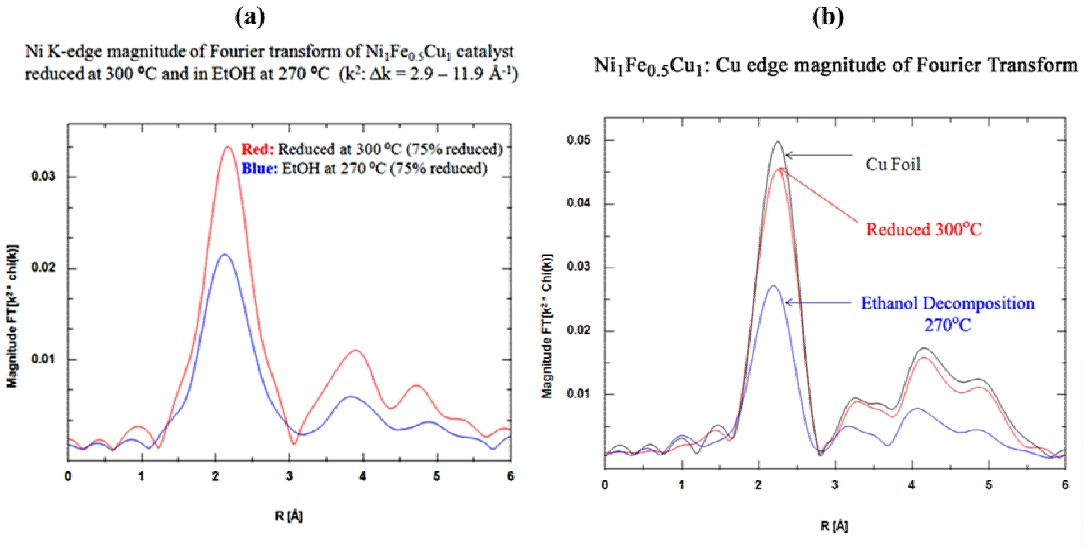

470

471

Figure 6: (a) Ni K-edge Fourier transform of the $Ni_1Fe_{0.5}Cu_1$ catalyst after reduction at 300ºC and during ethanol decomposition at 270ºC. (b) Cu K-edge magnitude of Fourier transform of $Ni_1Fe_{0.5}Cu_1$ catalyst reduced at 300 ºC and in EtOH at 270ºC (k^2: $\Delta k = 2.7 – 10.7$ Å^{-1})

471 None of the Fe containing catalysts show any metallic Fe in any of the conditions used, be
472 in air, reduced, or under reaction. Direct fitting of Fe XANES edge was not generally successful
473 compared with any of the reference samples and we lacked a $NiFe_2O_4$ reference that could have
474 provided a better fit.

475 XANES spectra of Fe oxide standards (FeO, Fe_2O_3 and Fe_3O_4) showed that the edge
476 energy shifts linearly toward higher values with increasing oxidation state of Fe (Fig. S3a). The
477 edge energy is linearly dependent on the oxidation state of the iron oxide samples as determined

by a sharp peak in first derivative of the edge, with oxidation state (figure S3b). This information was used to determine the average oxidation state of Fe in the samples (Table S3), which changes slightly upon reduction with H_2 at 300ºC, however, Fe is not completely reduced to FeO or metallic Fe in any of the samples and conditions used.

It should be noted that the particles size suggested by XAFS are smaller than what is displayed in the TEM image in figure 4. In Fig 4 a large particle was selected to obtain a compositional map displaying the inhomogeneity at nanoscale and its size is not a statistically average. The information obtained by XAFS is representative of a larger volume average value from a sample volume determined from the beam diameter of 3 mm averaged at the mesophase scale. Furthermore, since the particle is composed of multiple oxides, the XAFS particle size is only an approximate estimation based on the metal fraction present in nanoparticles.

The XAS results discussed so far for $Ni_1Fe_{0.5}Cu_1$ catalyst can be summarized as follows:

1) Ni was observed to be present giving 25% Ni(II) and 75% Ni(0) after reduction. Ni oxidation state does not change during the ethanol decomposition reaction, however, it gets oxidized to 30% Ni(II) and 70% Ni(0) during ethanol partial oxidation reaction. Formation of mixed Cu-Ni phases is also possible.

2) Cu in $Ni_1Fe_{0.5}Cu_1$ catalyst in air is 25% Cu(I) and 75% Cu(0). During reduction in H_2 at 300^{o}C, it gets completely reduced to metallic Cu(0). During reaction, apart from pure Cu metal nanoparticles, there is 15% Cu(I) during ethanol decomposition, which increases to 30% Cu(I) during ethanol partial oxidation. Particle size decreases from large sizes after reduction to 3 nm during ethanol decomposition and ethanol partial oxidation reactions.

3) Direct XANES fitting of Fe edge was not generally successful, however qualitatively no metallic Fe was observed in the spectra and the oxidation state did not seem to be affected by the reaction conditions.

The XPS and XAFS results were helpful in analyzing the surface and bulk concentration of each element respectively as well as their oxidation states in different environmental conditions. These techniques are effective in providing insights involving the reorganization of the catalytic particles such as the rearrangement on the surface to minimize surface energy, and change in oxidation state and size under reaction conditions. Because the technique operate in different environments (UHV RT vs operando) the results are not the same but rather complementary. Furthermore, the volume sampled in each case is different (surface vs bulk) which will give similar results only if the catalyst are highly dispersed on a support and the XAS signal are coming mainly from surface atoms. On the other hand the presence of the support presents additional challenges to get a good signal/noise ratio.

3.5 Fourier Transform Infrared Spectroscopy:

FTIR studies were conducted to obtain information about the adsorbed intermediates on the catalyst surface, and to be able to correlate them to the various oxidation states observed by XAS studies.

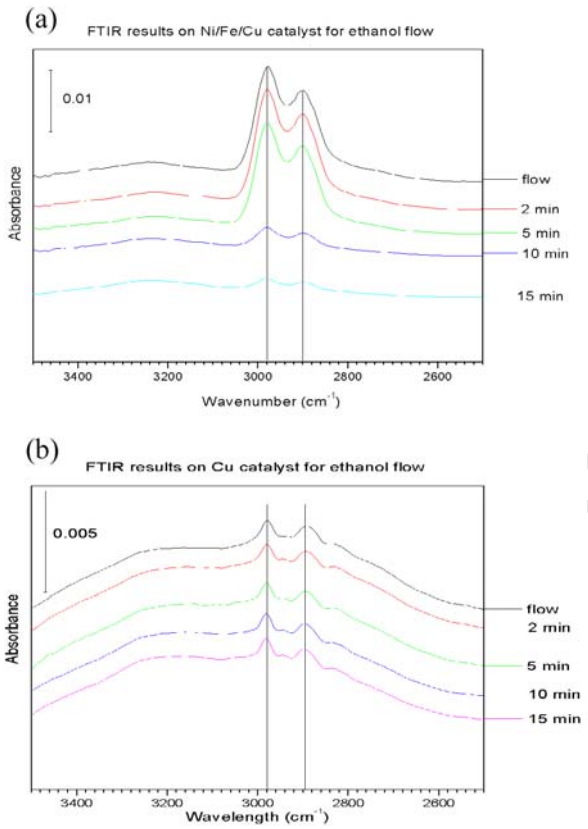

516 Fig. 7. In situ DRIFTS spectra of (a) $Ni_1Fe_{0.5}Cu_1$ and (b) Cu only catalysts during ethanol
517 desorption at room temperature and various times.
518
519 Figure 7-a, 7-b show the results obtained during ethanol desorption studies on
520 $Ni_1Fe_{0.5}Cu_1$ catalyst as well as on Cu only catalyst. To adsorb ethanol on the catalysts, a helium
521 stream saturated with ethanol was fed into the IR cell over the diluted catalysts for about 10 min
522 at room temperature. Then the cell was purged with pure He flow while recording the spectra at
523 various time intervals. The cell was modified to minimize the space between the window and
524 sample (~ 1mm) and reduce the signal from gaseous ethanol and ensure that most of the signals
525 are due to diffused reflectance from the catalyst's surface and not from the gas phase. As
526 displayed in fig 7a, the intensity of the band corresponding to C—H stretching frequency (2800-

3000 cm^{-1}) decreases rapidly with time on $Ni_1Fe_{0.5}Cu_1$ catalyst, but, on Cu the peak intensity, albeit smaller, remains almost constant throughout the selected time period of 15 minutes. If the C—H band is associated with adsorbed ethanol or an ethoxy intermediate, these results would indicate that such species is more stable on the Cu surface than on $Ni_1Fe_{0.5}Cu_1$. Fig. S3 (supplementary section) shows a wide wavelength range spectrum (wavelength: 700 cm^{-1} – 4000 cm^{-1}) exhibiting bands for ethanol on $Ni_1Fe_{0.5}Cu_1$ catalyst. All the peaks associated with the ethoxy intermediate and the adsorbed ethanol molecule decrease proportionally with time suggesting that the adsorbed species desorb quickly rather than participating in a reaction. The formation of ethoxy species has been reported previously on Cu [27], Fe [28] and on Ni [29, 30] surfaces. Ethoxy species have also been reported in the literature to be more stable on Cu and Fe surfaces whereas they are unstable on Ni surfaces forming methane, CO, hydrogen and surface carbon by breaking of C—H and C—C bonds [29]. The increase in the rate of desorption in the presence of Ni and Fe could be due the instability of ethoxy species on Ni sites.

The complete in-situ DRIFT spectra on the catalyst in a continuous flow of ethanol saturated He stream were collected at different temperatures on $Ni_1Fe_{0.5}Cu_1$ catalyst (fig. 8). The spectra obtained were smoothed using ORIGIN data analysis and a graphing software by applying the Savitzky-Golay method with 20 points of windows. A number of IR bands are observed which vary with temperature. Based on the literature results quoted, the bands observed at different temperatures can be ascribed to the following species: the bands at 720-785 cm^{-1} correspond to —$(CH)_n$— rocking vibrations for n=1-4, and bands at 970-1250 cm^{-1} can be related to ethanol C—O stretching frequencies whereas bands at around 1640 indicate the presence of un-dissociated water [31]. The band corresponding to C—H stretching between 2800-3000 cm^{-1} for CH_2, CH_3, and 1350-1470 cm^{-1} for bending CH_2, CH_3 and 860-880 cm^{-1} [32]

for CCO indicate the presence of ethoxy species on the surface. IR bands around 1550-1560 cm^{-1} indicate formation of some acetate species as well as some carbonate species (1505 cm^{-1}). The bands at 1720-1740 cm^{-1} and at 1400-1450 cm^{-1} has been ascribed to CO and to CH_2 bending in aldehydes indicating the presence of acetaldehyde formation, which become more visible at temperatures (T) above 200ºC. At T = 350ºC, two extra peaks between 2700-2750 cm^{-1} appear corresponding to the absorption of —CHO group. The bands at around 3700 cm^{-1} correspond to the O—H bond stretching in ethanol and water molecules and their intensities vary with temperature.

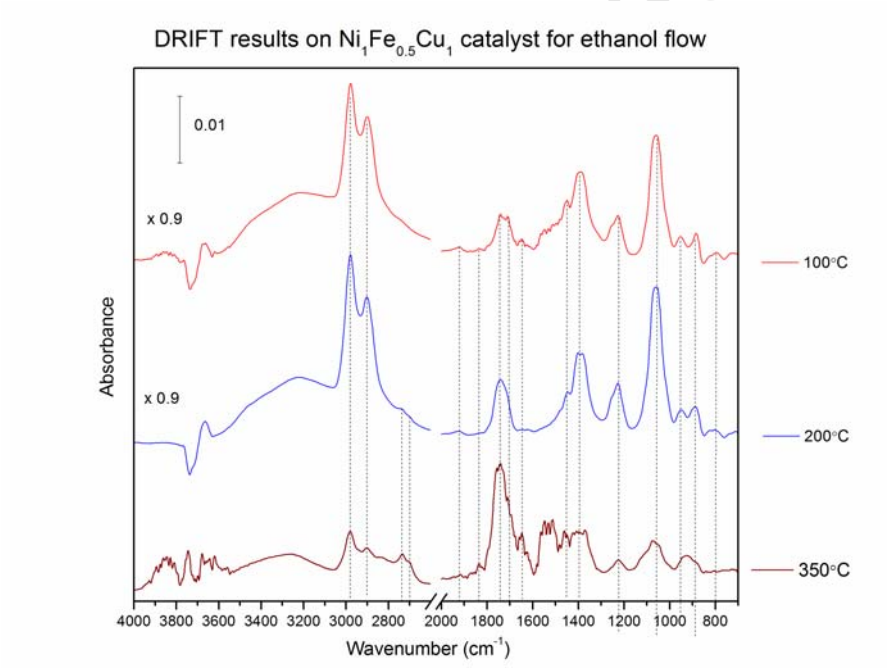

Figure 8: DRIFT studies for ethanol decomposition on $Ni_1Fe_{0.5}Cu_1$ catalyst

Based on the DRIFT results, the ethanol decomposition reaction involves the adsorption of ethanol molecule on the catalyst surface through its OH group to the active site. Afterwards ethoxy species (—OCH_2CH_3) are formed on the surface of the catalyst, as reported on different

surfaces by other authors [27, 28, 30, 32-36]. The adsorbed ethoxy species can lose one hydrogen atom to form acetaldehyde or it can gradually lose more hydrogen atoms by sequential CH bond scission. Ethanol adsorbed on the different phases present on the $Ni_1Fe_{0.5}Cu_1$ multicomponent catalyst involves interactions with the different metals. The ethoxy species on the Cu surface can undergo further decomposition to form acetaldehyde and hydrogen [27], which seems to be the active phase at low temperature where acetaldehyde appears as the dominant selective product [14]. On the Ni surface, the ethoxy specie is relatively unstable and breaks down to give methane, carbon monoxide and carbon [29]. Benziger et. al [28] reported the formation of stable ethoxy on Fe surface where it converts into CO and H_2. Fe is an active catalyst for Fischer-Tropsch synthesis [37-39], and it is likely to favor higher alkane formation. While Fe oxides are mostly detected by XAS, given the complexity of some particles, as shown in Fig 4, we cannot rule out the presence of small surface iron or surface iron carbide phases undetected by XAS. These observations are in agreement with our previously reported results that Ni is more selective for CH_4 production whereas Fe is selective for ethane formation [14]. The difference in the behavior of Ni and Fe could be understood by the fact that Ni mainly produces CH_4 whereas Fe is more selective for higher alkanes and alcohols under CO hydrogenation reaction [40, 41]. So the formation of ethoxy as an intermediate species as implied from FTIR and its subsequent decomposition to different products is consistent with our selectivity results [14].

Table 2 summarizes activity-selectivity results of ethanol decomposition at 50% conversion on the $Ni_1Fe_{0.5}Cu_1$ and on Ni, Fe and Cu only catalysts along with the corresponding temperature and selectivity for the products listed. The results vary with temperature, with most catalysts exhibiting 90-100 % conversion at temperatures above 450^{o}C and hydrogen selectivity

586 reaching about 40% [14]. Table 3 gives the activity, hydrogen selectivity and the reaction rate at

587 200^0C for the optimized catalyst and on the monometallic catalysts. It is clear that the

588 $Ni_1Fe_{0.5}Cu_1$ is the most active one giving 42% conversion and 20% hydrogen selectivity as
589 compared to individual metals Ni, Fe and Cu giving 29%, 11%, 16% conversion and 24%, 13%,
590 16% hydrogen selectivity respectively. The reaction rate is highest ~0.04 mol/min/g-cat on the
591 optimized catalyst. The above results can be summarized as following [14]:

592 • Cu is mainly selective for CH_3CHO and H_2
593 • Ni is selective for CH_4, H_2, H_2O and carbon
594 • Fe showed selectivity towards CO_2, C_2H_6, H_2 and carbon

595 The optimized $Ni_1Fe_{0.5}Cu_1$ catalyst is selective towards formation of different compounds in
596 different temperature ranges:

597 • An increasing trend in CH_3CHO and H_2 selectivity till temperature < 250ºC
598 • An increase in CH_4 and H_2 selectivity whereas a decrease in CH_3CHO selectivity in the
599 temperature range of 250ºC < T < 380ºC
600 • An increase in CH_4, H_2 and CO_2 selectivity for temperatures > 380ºC.

601

Table 2: Temperature of 50% ethanol conversion (T_{50}) and selectivities on Ni, Fe, Cu catalysts

Catalyst	Temperature of 50% conversion (T_{50})	CH_3CHO-selectivity at T_{50} (%)	H_2-selectivity at T_{50} (%)	CO_2-selectivity at T_{50} (%)	CH_4-selectivity at T_{50} (%)	C_2H_6-selectivity at T_{50} (%)
$Ni_1Fe_{0.5}Cu_1$	214	65	23	0	3	0
Ni	233	6.3	30.6	0	47.4	0.5
Fe	309	46.7	35.3	11.5	0	0.9
Cu	265	90.5	31.2	0	0	0

Table 3: Comparison of reaction rate, conversion and hydrogen selectivity in different catalysts at 200^0C

	Temperature 200^0C		
Catalyst	Reaction rate (mol/min./gm-catalyst)	Conversion (%)	H_2 selectivity (%)
$Ni_1Fe_{0.5}Cu_1$	0.03908	42	20
Ni	0.0273	29	24
Fe	0.0103	11	13
Cu	0.0152	16	16

The combined characterization techniques and activity results indicate that the role of individual phases on the $Ni_1Fe_{05}Cu_1$ catalyst during ethanol decomposition reaction at various

temperatures correlate with product formation as shown in Scheme 1. The Cu and Fe surfaces form stable ethoxy species upon ethanol adsorption. At lower temperature (<250ºC), Cu(0) is more active and produces CH_3CHO as main product. The Ni(0) sites break the C—H and C—C bonds of adsorbed ethoxy to form hydrogen, methane and CO, reducing the CH_3CHO concentration at temperatures in the 250ºC-380ºC range. Ni(0) possibly prevent Fe from forming long chain alkanes by Fischer-Tropsch synthesis. Ni(0) and Fe (Fe(II), Fe(III)) seem to be active at higher temperature (>380ºC) as CH_4 and CO_2 along with H_2 are the main products in this temperature range. The following reaction pathway is proposed to interpret the activity results in the multicomponent catalysts based on the in-situ characterization results.

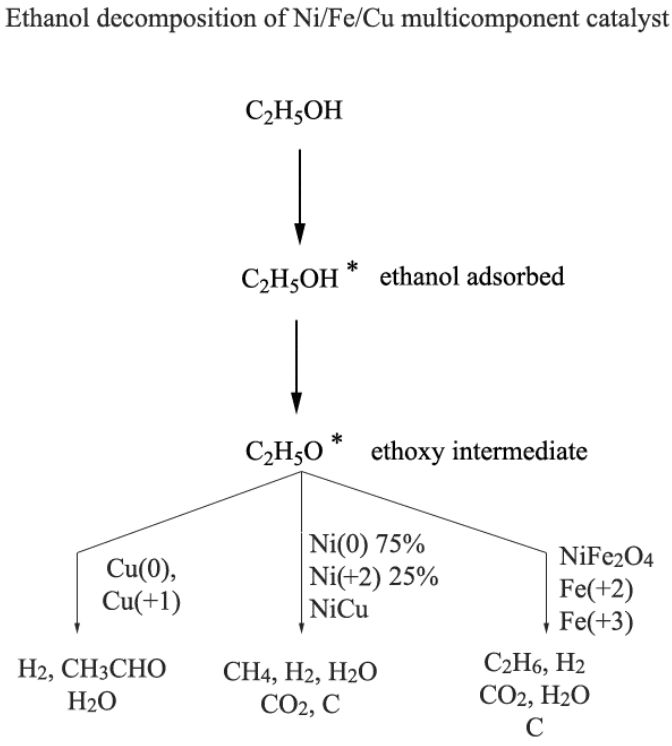

Scheme 1: Proposed reaction sequence and active phases in the ethanol decomposition reaction on $Ni_1Fe_{0.5}Cu_1$ catalyst

4 Summary:

A multicomponent catalyst $Ni_1Fe_{0.5}Cu_1$ used for ethanol decomposition and partial oxidation of ethanol has been characterized using different analytical tools. The XRD result suggests that the combustion of the precursor solution leads to the formation of NiCu and $NiFe_2O_4$ spinel phases. The Ni, Cu and Fe metals when present together exhibit a synergistic effect to form a more reducible $Ni_1Fe_{0.5}Cu_1$ catalyst than the individual metal oxides themselves as shown by TPR results. Changes in surface composition and structure occurs during reduction. XPS spectra indicate that the surface atomic ratio in air is Ni:Fe:Cu 1:1.3:2 in air, and it changes upon reduction to give a Ni:Fe:Cu ratio of 1:2.4:2.6, but the surface regains its initial surface composition when exposed to air after the reaction. Ni and Cu are present in partially reduced form after synthesis and exposure to air, but are further reduced in H_2 at 300ºC, whereas Fe is not much affected by the reduction process and remains mainly in oxidized form at that temperature. Carbon formation is also observed on the surface after reaction. SEM images indicate that carbon has a filament like structure - of about 25-50nm diameter. The HRTEM images indicate that different phases are segregated at nanosclale, partially explaining the gradual shift in the selectivity with change in temperature. XAS studies show that Cu in $Ni_1Fe_{0.5}Cu_1$ is 25% Cu_2O and 75% metallic Cu at room temperature. Cu is completely reduced in H_2 at 300ºC and shows 15% Cu_2O and 85% metallic Cu during ethanol decomposition reaction at 270ºC whereas 30% Cu_2O and 70% metallic Cu at 270ºC during ethanol oxidative reforming. Fe however is only slightly affected by reduction at 300ºC and always shows an oxidation state above 2.3. No metallic Fe was observed in any of the treatments used. Ni is 75% reduced at 300 ºC in presence of H_2 and maintains the same oxidation state during ethanol decomposition at 270 ºC, however it gets partially oxidized to 70% metallic Ni during ethanol partial oxidation reaction at 270ºC.

646 It should also be notes that because the different characterization techniques used sample
647 different populations of catalytic particles (nanosize to micron size) and each operates at
648 different conditions (air, H_2, UHV, under reaction) and they have different penetration depth
649 (near surface to bulk), currently it is not possible to identify the specific sites involved at the
650 different conditions but only ascertain in general the phases involved to explain the trends
651 observed.

652 **Acknowledgements:** We gratefully acknowledge funding from NSF Grant 0730190 for support
653 of this work. This work was also partially supported by Notre Dame Integrated Imaging Facility.
654 Use of the Advanced Photon Source is supported by the U. S. Department of Energy, Office of
655 Science, and Office of Basic Energy Sciences, under Contract DE-AC02-06CH11357.
656

656 *References*

657 *[1] K.C. Patil, M.S. Hegde, R. Tanu and S.T. Aruna, Chemistry of Nanocrystalline Oxide*
658 *Materials : Combustion Synthesis, Properties and Applications, World Scientific Publishing Co.*
659 *Pte. Ltd, Singapore, 2008.*

660 *[2] S.T. Aruna and A.S. Mukasyan, Current opinion in solid state materials science 12 (2008)*
661 *44.*

662 *[3] J. J. Kingsley, K. C. Patil, Materials letters 6 (1988) 427.*

663 *[4] A.G. Merzhanov, I.P. Borovinskaya and A.E. Sytchev, in: Baumard J F (Ed.), Lessons in*
664 *Nanotechnology from Traditional Materials to Advanced Ceramics, Techna Group Srl, Dijon,*
665 *France, 2005, pp. 1-27.*

666 *[5] S. Schuyten, E. E. Wolf, Catalysis Letters 106 (2006) 7.*

667 *[6] L. Shi, K. Tao, R. Yang, F. Meng, C. Xing and N. Tsubaki, Applied Catalysis A: General 401*
668 *(2011) 46-55.*

669 *[7] C. H. Jung, H. G. Lee, C. J. Kim, S. B. Bhaduri, Journal of nanoparticle research 5 (2003)*
670 *383.*

671 *[8] C. H. Jung, S. Jalota, S. B. Bhaduri, Mater Lett 59 (2005) 2426.*

672 *[9] A. Kumar, E. Wolf, A. Mukasyan, AIChE Journal 57 (2010) 2207.*

673 *[10] A. Kumar, E. Wolf, A. Mukasyan, AICHE Journal 57 (2011) 3473 .*

674 *[11] A. S. Mukasyan, P. Dinka, Advanced engineering materials 9 (2007) 653.*

675 *[12] A. Kumar, E. Wolf, A. Mukasyan, Applied catalysis.A, General 372 (2010) 175-183.*

676 *[13] A. Kumar A.S. Mukasyan, E.E. Wolf, Industrial engineering chemistry research 49 (2010)*
677 *11001-11008.*

678 *[14] A. Kumar, A. Mukasyan and E. Wolf, Applied Catalysis A: General 401 (2011) 20-28.*

679 *[15] K. Öhgren, A. Rudolf, M. Galbe, G. Zacchi, Biomass Bioenergy 30 (2006) 863.*

680 *[16] Y. Sun, Bioresour. Technol. 83 (2002) 1.*

681 *[17] B. Grant, Introduction to XAFS : a practical guide to X-ray absorption fine structure*
682 *spectroscopy, Cambridge, UK ; New York : Cambridge University Press, Cambridge, UK ; New*
683 *York, 2010.*

684 *[18] L. Vitos, A.V. Ruban, H.L. Skriver and J. Kollar, Surface Science 411 (1998) 186-202.*

685 *[19] A. Navrotsky, C. Ma, K. Lilova and N. Birkner, Science 330 (2010) 199.*

686 *[20] R.T.K. Baker, Carbon 27 (1989) 315-323.*

687 *[21] M. Kumar and Y. Ando, Journal of nanoscience and nanotechnology 10 (2010) 3739.*

688 *[22] K.J. MacKenzie, O.M. Dunens and A.T. Harris, Industrial engineering chemistry research*
689 *49 (2010) 5323.*

690 *[23] A.C. Dupuis, Progress in Materials Science 50 (2005) 929.*

691 *[24] A. Jentys, PCCP.Physical chemistry chemical physics 1 (1999) 4059.*

692 *[25] B.J. Kip, F.B.M. Duivenvoorden, D.C. Koningsberger and R. Prins, Journal of catalysis*
693 *105 (1987) 26.*

694 *[26] B.S. Clausen, L. Grabaek, H. Topsoe, L.B. Hansen, P. Stoltze, J.K. Norskov and O.H.*
695 *Nielsen, Journal of catalysis 141 (1993) 368.*

696 *[27] M. Bowker, Surf. Sci. 116 (1982) 549.*

697 *[28] J.B. Benziger, Journal of catalysis 65 (1980) 36.*

698 *[29] S.M. Gates, J.N. Russell Jr. and J.T. Yates Jr., Surf. Sci. 171 (1986) 111-134.*

699 *[30] J. Xu, Surf. Sci. 256 (1991) 288.*

700 *[31] T. Tabakova, Applied catalysis.A, General 252 (2003) 385.*

701 *[32] M.A. Natal Santiago, Journal of catalysis 175 (1998) 252.*

702 *[33] T. Iwasita, Electrochim. Acta 39 (1994) 531.*

703 *[34] G. Blyholder, J. Phys. Chem. 70 (1966) 1745.*

704 *[35] W. Cai, F. Wang, E. Zhan, A.C. Van Veen, C. Mirodatos, W. Shen, Journal of catalysis 257*
705 *(2008) 96.*

706 *[36] H. Song, Journal of molecular catalysis.A, Chemical 318 (2010) 21.*

[37] P. Moodley, F. Scheijen, J. Niemantsverdriet and P. Thüne, Catalysis Today 154 (2010) 142-148.

[38] H. Dong, M. Xie, J. Xu, M. Li, L. Peng, X. Guo and W. Ding, Chemical Communications 47 (2011) 4019-4021.

[39] H. Zhao, Q. Zhu, Y. Gao, P. Zhai and D. Ma, Applied Catalysis A: General 456 (2013)233-239.

[40] Storch H. H., Golumbic N. and Anderson R. B., The Fischer Tropsch and related SynthesesNew York, 1951.

[41] Anderson R. B. (Ed.), CatalsisReinhold, New York, 1956.